JOURNAL OF GREEN COMPLEX ENGINEERING, 2026, Vol.4, No.1, 79~88
https://doi.org/10.59810/greenplexresearch.v4i1.294
e-ISSN 3025-9673

A cross-validated discharge–grain-size model for maximum bed scour in a mobile-bed open channel

Soemitro Emin Praja[1]*, M. Nurhidayat[1], M. Agusalim[2], Asran[3]

[1]Urban and Regional Planning Program, Faculty of Engineering, Universitas Muhammadiyah Makassar, Makassar, Indonesia

[2]Department of Water Resources Engineering, Faculty of Engineering, Universitas Muhammadiyah Makassar, Makassar, Indonesia

[3]Safety Engineering Study Program, Tri Tunas Nasional Institute of Technology and Health, Makassar, Indonesia

ABSTRACT

This study develops a compact empirical model for maximum bed scour in an unobstructed mobile-bed open channel. Experiments were conducted in a 9 m flume using a 3×3 matrix that combined discharges of 0.0026, 0.0034, and 0.0045 $m^3 s^{-1}$ with nominal grain sizes of 2.36, 1.18, and 0.85 mm. Final bed change was measured at 20 sections and seven transverse points for each condition, providing 1,260 spatial observations. Maximum scour increased from 0.8 to 4.5 cm, while the proportion of scoured observation points rose from 19.3% to 100%. The additive relation d_s(cm)=1.272+0.883Q*−1.037d* explained 93.5% of the fitted variance and retained R^2=0.843 under leave-one-condition-out cross-validation, with RMSE=0.394 cm. A particle-densimetric-Froude formulation produced a very strong fit on the normalized response scale but only a marginal reduction in cross-validated error after back-transformation. Discharge and grain size therefore acted as comparably strong controls in opposite directions within the tested range. The proposed relation is intended for interpolation within this experimental domain rather than as a universal design equation.

ARTICLE HISTORY

Received June 25, 2026
Received in revised form July 26, 2026
Accepted August 20, 2026
Available online August 28, 2026.

KEYWORDS

bed scour; mobile-bed channel; discharge; grain size; cross-validation

1. Introduction

Mobile beds adjust whenever the hydraulic forces acting at the sediment–water interface become large enough to entrain, translate, or suspend grains. The resulting response is not limited to a change in bed elevation at one point: it may involve a redistribution of sediment over the reach, a shift from local deposition to generalized degradation, and the development or migration of bedforms. Field evidence shows that sediment deficits and altered flow regimes can accelerate downstream channel deformation, while flood magnitude can control the spatial extent of incision in steep alluvial channels [1,2]. Numerical studies of erodible channels similarly represent flow and sediment continuity as a coupled system in which hydraulic state and bed elevation evolve together [3-5]. These studies establish the broader morphodynamic setting for the present work: maximum scour is an outcome of a distributed flow–sediment interaction rather than an isolated geometric quantity.

For a non-cohesive bed, discharge and particle size provide two direct ways of changing that balance. Increasing discharge generally raises the capacity of the flow to do work on the bed, whereas increasing grain size increases particle resistance and can alter packing, exposure, and surface roughness. Recent studies show that sediment characteristics influence transport capacity [6], that non-uniform particle distributions modify sediment organization in open-channel flow [7], and that erosion thresholds in sand–silt mixtures vary with composition and hydraulic state [8,9]. Channel-scale experiments also demonstrate that armoring, roughness, and grain-size uniformity modify the stability of an erodible surface [10,11]. Nominal diameter is therefore a useful experimental control, but it should not be mistaken for a complete description of sediment resistance.

The near-bed mechanism is further complicated by turbulence and three-dimensional flow organization. In open-channel confluences, secondary circulation and organized near-bed motion can focus erosion even when bulk flow variables appear modest [12]. Numerical work shows that discharge ratios alter vorticity and mixing structures that can promote mid-channel scour [13], while measurements over mobile dunes associate high Reynolds shear stress and coherent sweep or ejection events with active sediment entrainment and bedform migration [14,15]. Direct experimental observations likewise link turbulent structure to the developing scour topography [16] and show that suspended-sediment pathways in confluences have substantial three-dimensional structure [17]. A model based only on discharge and grain size cannot resolve these processes, but it can provide a transparent baseline against which their additional explanatory value can later be tested.

Much of the contemporary scour literature addresses local scour produced by a discrete obstruction. Bridge piers, abutments, spur dikes, longitudinal walls, and buried infrastructure generate separation, downflow, horseshoe vortices, and wake structures that differ fundamentally from distributed boundary forcing over an unobstructed reach. Laboratory studies have demonstrated strong geometry effects for tandem piers and spur dikes [18,19], and countermeasure studies show that changes in local flow structure can substantially reduce scour around abutments and training walls [20,21]. Grain-size distribution and pier geometry also affect the depth and position of local scour

CONTACT: Soemitro Emin Praja soemitroeminpraja.ft@unismuh.ac.id Urban and Regional Planning Program, Faculty of Engineering, Universitas Muhammadiyah Makassar, Makassar, Indonesia

[22], while controlled cable-burial experiments show an increase in scour rate with increasing flow intensity across several sediment sizes [23].

Recent laboratory work provides a useful comparison while reinforcing this distinction. In open-channel pier experiments, greater discharge was accompanied by greater unprotected scour, whereas porous underwater deflectors reduced near-bed velocity and scour depth [24]. A companion study quantified substantial reductions in mean velocity after installation of a reinforced porous cylindrical deflector [25]. These findings support the physical importance of discharge and velocity, but their response is structure-induced. The present experiment contains no pier, abutment, culvert, or deflector in the measurement reach. Its purpose is therefore different: to isolate the coupled influence of discharge and nominal grain size on maximum scour generated by an unobstructed mobile bed.

A second question concerns how much model complexity is justified by a small factorial experiment. Coupled depth-averaged and meshless sediment models can reproduce erosion and bed evolution under rapidly varying flow [3,26], while inverse modeling and data assimilation can improve representation of movable-bed hydraulics when richer observations are available [27,28]. Physically informed dimensional reduction has also been proposed as a way to retain interpretability before applying high-flexibility predictive methods [29]. In parallel, scour-prediction studies increasingly use external or holdout validation rather than reporting fitted R^2 alone [30,31]. For the present nine-condition matrix, this literature argues for a deliberately low-parameter model and a validation scheme that respects the treatment structure of the experiment.

The available dataset contains 140 final bed-elevation observations for each of nine discharge–grain-size combinations. Those 1,260 spatial values describe bed morphology in detail, but they do not constitute 1,260 independent treatment replications because each set of 140 points shares a common run and hydraulic history. The statistical unit for a maximum-scour model is therefore the experimental condition, not the individual bed point. This distinction is important in small flume studies: dense spatial sampling improves description of morphology, whereas predictive uncertainty still depends on the number of independent hydraulic treatments. The analysis consequently uses the nine conditions for model estimation and leave-one-condition-out cross-validation, while the full spatial grid is retained to describe the expansion of degradation across the bed.

The study has four objectives. First, it quantifies maximum scour and the proportion of scoured observation points across the 3×3 experimental matrix. Second, it examines end-of-run hydraulic descriptors to determine whether changes in flow regime accompany the bed response. Third, it estimates an additive discharge–grain-size model and compares it with a multiplicative power relation and a particle-densimetric-Froude formulation. Fourth, it evaluates predictive stability through leave-one-condition-out cross-validation and a source-data audit. The working hypothesis is that maximum scour increases with discharge and decreases with grain size, with both effects remaining identifiable when estimated simultaneously. A related hypothesis is that normalization by grain size and Fr_p will reduce part of the apparent two-factor structure. The contribution is a compact, testable baseline for an unobstructed mobile bed, together with explicit limits on the interpretation of a model derived from only nine independent conditions.

2. Methods

2.1 Experimental facility and design

The experiments were conducted in the Hydrology Laboratory, Faculty of Engineering, Universitas Muhammadiyah Makassar. The physical model was a 9.00 m open-channel flume with a bed width of 0.30 m and a channel height of 0.40 m. The working bed consisted of a nominal 0.10 m layer of non-cohesive granular material. Before each run, the channel was cleaned, the sediment layer was levelled, and the hydraulic system was operated to establish the prescribed discharge. The source documentation describes a recirculating arrangement with upstream and downstream storage and an energy-dissipation section.

A complete 3×3 matrix crossed three discharges, Q=0.0026, 0.0034, and 0.0045 $m^3\ s^{-1}$, with three nominal sediment diameters, d=0.00236, 0.00118, and 0.00085 m. The sediment density used in the reconstructed calculations was approximately 2,650 kg m^{-3}, and water density was taken as 1,000 kg m^{-3}. Each condition was maintained for 24 min (1,440 s). Mean velocity and water depth were observed at 480, 960, and 1,440 s; the final bed surface was measured after shutdown and drainage. No independent repeat runs are documented for each cell of the factorial matrix. The nine discharge–grain-size combinations are therefore treated as the independent experimental units for model development.

2.2 Bed-change reconstruction and response variables

For each condition, final bed-elevation change was recorded at 20 longitudinal sections and seven transverse observation points, giving 140 values per run and 1,260 values across the full matrix. The original sign convention was preserved: negative values indicate degradation, positive values indicate deposition, and zero indicates no measured change. Maximum scour depth, d_s, was defined as the absolute value of the most negative bed-elevation change in each condition, $d_s=|\min(\Delta z)|$. Maximum deposition, mean bed change, the number of negative, positive, and unchanged points, and the percentage of scoured observation points were also recalculated from the 140 values.

Maximum scour and spatial prevalence were kept as separate descriptors. The maximum is an extreme statistic that identifies the deepest measured degradation but is sensitive to one observation point. The scoured-point percentage indicates how widely negative bed change is distributed over the measurement grid. Because the physical area represented by each point was not documented well enough for rigorous areal weighting, this percentage is interpreted only as the fraction of sampled locations that experienced scour. It is not reported as an eroded-area percentage or a volumetric sediment balance.

2.3 Hydraulic descriptors and candidate models

End-of-run hydraulic descriptors at t=1,440 s included mean velocity V, water depth h, Froude number Fr, and Reynolds number Re. The source-calculated Fr and Re values were retained because the available documentation does not preserve every intermediate hydraulic-geometry convention needed to reproduce them unambiguously. Their reported ranges were 0.819–1.400 for Fr and approximately 5.12×10^4–1.16×10^5 for Re. The particle densimetric Froude number, Fr_p, was recomputed from quantities available consistently across the nine conditions as $Fr_p=V/[g((\rho_s-\rho w)/\rho w)d]^{1/2}$, where $g=9.81$ m s^{-2}, $\rho_s=2{,}650$ kg m^{-3}, $\rho w=1{,}000$ kg m^{-3}, and d is nominal particle diameter. Boundary shear is an important driver of sediment motion in rectangular open channels [32], but the source shear calculations contained unresolved slope and classification inconsistencies; they were therefore excluded from the predictive models rather than used as uncertain derived inputs.

The primary model was an additive relation between maximum scour and the two experimentally controlled factors: $d_s(cm)=a+bQ^*+cd^*$, with $Q^*=Q/10^{-3}$ and $d^*=d/10^{-3}$. The scaling only changes coefficient interpretation. The discharge coefficient represents the change in maximum scour for a 0.001 m^3 s^{-1} increase in Q at fixed grain size, while the grain-size coefficient represents the change for a 1 mm increase in d at fixed discharge. A multiplicative alternative, $d_s(cm)=\alpha(Q^*)^\beta(d^*)^\gamma$, was estimated by ordinary least squares after log transformation. A third formulation used normalized scour, $d_s/d=A+BFr_p$. The latter was assessed both on the ratio scale and after predictions were converted back to centimetres because d occurs in both d_s/d and Fr_p and can therefore contribute shared mathematical structure to the fitted correlation. Similar caution about separating combined dimensionless effects from their component influences has been raised in mobile-bed scour analysis [33].

2.4 Validation, diagnostics, and data audit

Model performance was summarized with R^2, root mean square error (RMSE), mean absolute error (MAE), and mean absolute percentage error (MAPE). Adjusted R^2 was also calculated for the primary linear model. Predictive performance was evaluated by leave-one-condition-out cross-validation (LOOCV): each of the nine treatment combinations was omitted once, the model was fitted to the remaining eight conditions, and the omitted maximum scour was predicted. The pooled nine out-of-sample predictions were then used to calculate cross-validated R^2, RMSE, MAE, and MAPE. This procedure avoids a random split that would be unstable at n=9 and prevents the 140 within-run bed measurements from being treated as independent replicates.

For the additive model, conventional coefficient confidence intervals were accompanied by residual and influence screening. Residual normality was checked with the Shapiro–Wilk test, heteroscedasticity with the Breusch–Pagan test, collinearity with variance inflation factors, and influence with Cook's distance. A leave-one-condition-out coefficient sensitivity analysis recorded the fitted discharge and grain-size slopes in all nine refits. These diagnostics are interpreted descriptively because formal tests have limited power with nine observations. The intent is to identify obvious instability rather than to claim strong asymptotic inference.

A source-data audit preceded interpretation. Two pairs of 20×7 bed-change arrays are exact duplicates although they are assigned to different treatment combinations. Three narrative maximum-scour values also differ from the extrema contained in the corresponding tables, and the finest sediment is labeled 0.00085 and 0.00086 m in different locations. The analysis follows the numerical bed-change tables, uses 0.00085 m consistently for the finest nominal diameter, and excludes the disputed shear-stress chain. These conventions preserve a reproducible analytical path while acknowledging that corrected laboratory records could change the numerical coefficients. The audit is therefore part of the model's uncertainty statement, not a post hoc editorial adjustment.

3. Results and Discussion

3.1 Hydraulic regime and spatial bed response

The end-of-run hydraulic measurements describe a consistent rise in flow intensity across the treatment matrix. For the coarsest bed (d=2.36 mm), mean velocity increased from 0.65 to 0.82 m s^{-1} as discharge rose from 0.0026 to 0.0045 m^3 s^{-1}. The corresponding range was 0.79–0.93 m s^{-1} for d=1.18 mm and 0.89–1.22 m s^{-1} for d=0.85 mm. Water depth varied more modestly, from 0.095 to 0.126 m. All reported Reynolds numbers were turbulent under the source classification. The reported Froude number increased from 0.819 in the low-discharge/coarse-bed condition to 1.400 in the high-discharge/fine-bed condition, so the matrix crosses from subcritical or near-critical flow into supercritical states. This transition is relevant because laboratory studies show that changes in Froude regime can accompany pronounced changes in flow organization and sediment-control performance; for example, a recent beam-type sabo-dam experiment reported systematic Froude changes as slope altered the hydraulic state [34]. In a different setting, Barahimi and Sui found Froude number to be an important control on maximum scour under open-flow conditions around vegetation elements [35].

Table 1 summarizes the nine treatment conditions and makes the coupled response visible. Maximum scour rose monotonically with discharge at every grain size and decreased monotonically with grain size at every discharge. The smallest value, 0.8 cm, occurred at Q=0.0026 m^3 s^{-1} and d=2.36 mm; the largest, 4.5 cm, occurred at Q=0.0045 m^3 s^{-1} and d=0.85 mm. The table also shows that the response was not limited to the single deepest point. The percentage of scoured observation locations increased from 19.3% in the least erosive condition to 100% in the most erosive condition. Figure 1 visualizes the same treatment structure: all three grain-size curves rise with discharge, while the finer-bed curves remain above the coarser-bed curve over the measured range.

Table 1. Experimental matrix, end-of-run hydraulics, and maximum-scour response.

Q (10^{-3} m³/s)	d (mm)	V (m/s)	h (m)	Fr	Re (×10^4)	Fr_p	d_s (cm)	Scoured points (%)
2.6	2.36	0.65	0.095	0.819	5.12	3.326	0.8	19.3
3.4	2.36	0.71	0.108	0.851	6.04	3.633	2.2	73.6
4.5	2.36	0.82	0.108	0.985	6.99	4.195	2.9	93.6
2.6	1.18	0.79	0.099	0.981	6.30	5.716	2.2	73.6
3.4	1.18	0.89	0.113	1.055	7.83	6.440	2.9	93.6
4.5	1.18	0.93	0.119	1.081	8.37	6.729	3.6	99.3
2.6	0.85	0.89	0.101	1.098	7.22	7.588	2.9	95.7
3.4	0.85	0.98	0.115	1.161	8.74	8.355	3.6	99.3
4.5	0.85	1.22	0.126	1.400	11.65	10.401	4.5	100.0

Note. Hydraulic variables are values at t=1,440 s; maximum scour and scoured-point percentages were recalculated from the 20×7 bed-change tables.
Source: experimental data

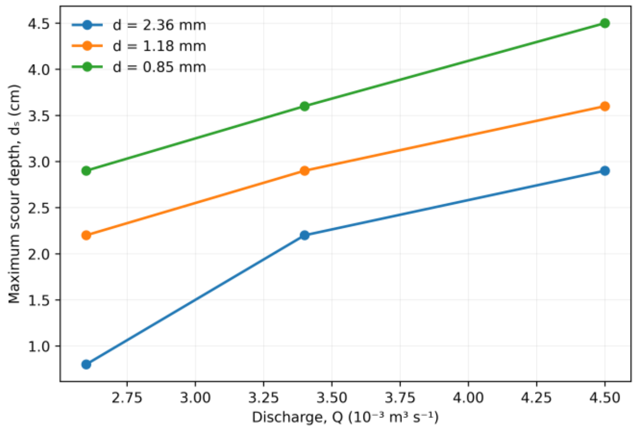

Figure 1. Maximum scour depth as a function of discharge for each nominal sediment grain size. Source: experimental data

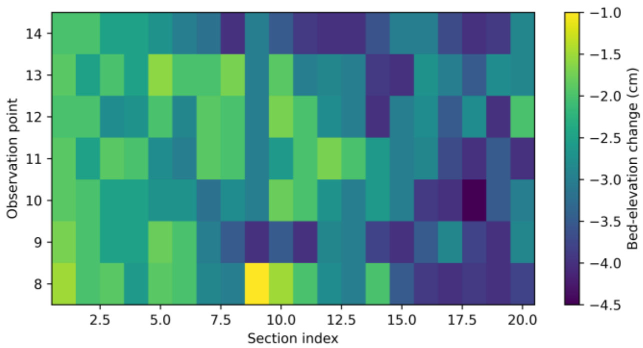

Figure 2. Bed-elevation change for Q=0.0045 m³ s⁻¹ and d=0.85 mm after 1,440 s. Negative values denote scour; the deepest tabulated value is −4.5 cm at section 18, observation point 10
Source: experimental data

The spatial statistics reveal a change in bed state rather than only a change in an extreme value. At Q=0.0026 m³ s⁻¹ and d=2.36 mm, 27 of 140 points were scoured, 89 showed deposition, and 24 were unchanged; the mean bed change was +0.419 cm. Increasing discharge to 0.0034 m³ s⁻¹ at the same grain size raised the scoured fraction to 73.6% and shifted the mean to −0.764 cm. At the highest discharge, 93.6% of the points were scoured and the mean change was −1.410 cm. Finer sediment produced the same shift at lower discharge. With d=0.85 mm and Q=0.0026 m³ s⁻¹, 95.7% of observations were already negative. Under Q=0.0045 m³ s⁻¹ and d=0.85 mm, all 140 observations showed degradation and the mean bed change reached −2.821 cm.

Figure 2 provides the two-dimensional view for that most erosive condition. The reconstructed surface is negative throughout the sampled grid, with the deepest tabulated value of −4.5 cm at section 18, observation point 10. The later section indices contain a cluster of relatively deep negative values, indicating that the maximum is embedded within a broader zone of degradation rather than appearing as an isolated outlier. This distinction matters when maximum scour is used as the modeled response. A point maximum can be sensitive to measurement spacing, whereas the spatial field shows whether the same condition also produces a coherent morphological response. High-resolution river monitoring has increasingly been used to capture this type of bedform and morphodynamic variability [36], and controlled alluvial-channel experiments show that evolving morphology may retain sensitivity to geometry and initial conditions [37].

The grain-size contrast was most pronounced in relative terms at low discharge. At Q=0.0026 m³ s⁻¹, reducing d from 2.36 to 0.85 mm increased maximum scour from 0.8 to 2.9 cm, a 262.5% rise. At Q=0.0045 m³ s⁻¹, the same grain-size contrast increased scour from 2.9 to 4.5 cm, or 55.2%. This does not establish a statistical Q×d interaction because independent run replication is absent, but it suggests that relative sensitivity is strongest near the low-forcing edge of the tested domain. Near-critical mobility experiments show that modest changes in local forcing can alter sediment-flux directionality [38], and fine sediment over a coarse bed can pass through distinct erosion regimes as sheltering and turbulence change [39]. The present pattern is therefore consistent with threshold-sensitive behavior even though the empirical model is intentionally linear on the centimetre scale.

3.2 Additive discharge–grain-size model

The additive fit to the nine condition-level maxima was d_s(cm)=1.272+0.883Q*−1.037d*, where Q*=Q/10^{-3} and d*=d/10^{-3}. The coefficient signs match the experimental hypothesis. Holding grain size constant, an increase of 0.001 m³ s⁻¹ in discharge corresponds to an estimated 0.883 cm increase in maximum scour. Holding discharge constant, a 1 mm increase in nominal grain size corresponds to an estimated 1.037 cm decrease. The model explained 93.5% of the observed variance (adjusted R^2=0.913), with an in-sample RMSE of 0.254 cm, MAE of 0.230 cm, and MAPE of 11.13%.

The standardized coefficients were +0.691 for discharge and −0.676 for grain size. Their similar absolute magnitudes are more informative than either raw coefficient alone because the predictors have different physical units. Within the experimentally covered ranges, neither factor behaves as a minor correction. The discharge span produces a scour response comparable in magnitude with the response generated by the 0.85–2.36 mm grain-size span. This balanced two-factor result is compatible with broader evidence that bed-material properties can be as important as hydraulic forcing in setting the morphological response. Hakim Safi and Mohapatra showed that bed material and downstream flow depth jointly influence bed evolution in an open-channel confluence [40], while numerical sheet-flow analysis demonstrates that grain size changes particle and fluid velocities as well as transport structure [41].

The positive discharge effect also agrees with the direction observed in structure-induced scour, without implying that the mechanisms are identical. Baharuddin et al. reported greater unprotected local scour at higher discharge around a cylindrical pier [24]. In the present unobstructed bed, the same direction emerges without a pier-generated horseshoe vortex. The implication is narrower: higher bulk forcing increased both the deepest measured degradation and the spatial prevalence of negative bed change. The model therefore captures a reach-scale treatment effect, not a transferable bridge-scour coefficient.

The negative grain-size coefficient should likewise be interpreted as an operational relationship within the tested material range. Field mapping of large rivers shows that grain-size patterns covary with transport conditions and spatial setting [42], while experiments and numerical work on non-uniform sediment emphasize that full gradation can materially affect model behavior [43]. The present coefficient consequently summarizes three nominal sieve-based treatments; it does not substitute for a gradation-dependent entrainment law. A stronger follow-up experiment should report full particle-size distributions, surface sorting, and any armoring that develops during the run.

Residual screening did not identify a gross departure from the additive model, but the sample size limits what can be inferred. The Shapiro–Wilk test gave $p=0.575$ and the Breusch–Pagan test $p=0.655$. Variance inflation factors were 1.00 because Q^* and d^* are orthogonal in the complete 3×3 design. The largest Cook's distance was 0.598 for the low-discharge/coarse-bed corner, greater than the common $4/n$ screening value. Importantly, omitting each condition in turn did not reverse either slope: the discharge coefficient ranged from 0.783 to 0.995 cm per 0.001 $m^3\,s^{-1}$, and the grain-size coefficient from −1.168 to −0.893 cm per millimetre. The exact coefficients remain uncertain, but the directional result is not created by one condition.

3.3 Cross-validation and comparison of candidate models

Figure 3 compares the observed maximum scour with the nine LOOCV predictions from the additive model. Each plotted prediction was generated by a model that did not include that treatment condition during fitting. The points remain close to the 1:1 line, but the spread is visibly larger than would be inferred from the fitted R^2 alone. Cross-validated R^2 was 0.843, with RMSE=0.394 cm, MAE=0.353 cm, and MAPE=18.24%. The increase in RMSE from 0.254 cm in sample to 0.394 cm under LOOCV is a direct estimate of calibration optimism. For a nine-condition dataset, that difference is scientifically more useful than presenting 0.935 as if it were an independent prediction statistic.

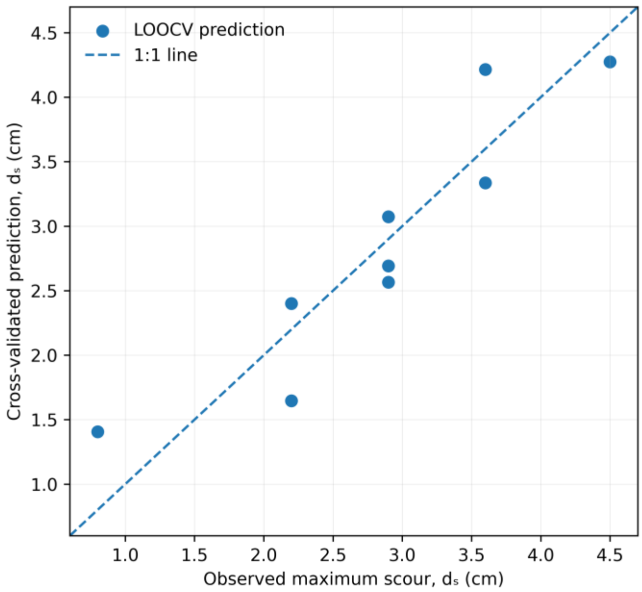

Figure 3. Observed maximum scour versus leave-one-condition-out cross-validated predictions from the additive discharge–grain-size model. The dashed line is the 1:1 line.
Source: experimental data and model results.

Table 2 places this result beside the two alternative formulations. The power model, $d_s(cm)=0.615(Q^*)^{1.345}(d^*)^{-0.724}$, retained physically plausible coefficient directions but had poorer performance: fitted $R^2=0.822$ and RMSE=0.419 cm, deteriorating to cross-validated $R^2=0.487$ and RMSE=0.713 cm. The additional multiplicative curvature therefore does not improve prediction in the available matrix. This result does not imply that scour is fundamentally additive outside the experiment. It indicates only that a more flexible response form is not supported strongly enough by nine treatment points to justify its extra sensitivity.

Table 2. In-sample and leave-one-condition-out performance of the candidate empirical models. Source: model results.

Model	Equation	R^2	RMSE (cm)	MAE (cm)	MAPE (%)	LOOCV R^2	LOOCV RMSE (cm)
Linear Q–d	$d_s=1.272+0.883Q^*-1.037d^*$	0.935	0.254	0.230	11.13	0.843	0.394
Power Q–d	$d_s=0.615(Q^*)^{1.345}(d^*)^{-0.724}$	0.822	0.419	0.361	15.89	0.487	0.713
Fr_p model	$d_s/d=-17.873+6.899Fr_p$	0.913†	0.293	0.258	13.49	0.850	0.385

Note. $Q^*=Q/10^{-3}$ and $d^*=d/10^{-3}$. †R^2 for the Fr_p model is reported after back-transformation to scour depth for dimensional comparability; the ratio-scale R^2 for d_s/d is 0.98

The preference for a parsimonious baseline is consistent with recent predictive work in hydraulic engineering. Large scour datasets can support more flexible ensemble or machine-learning models when training, testing, and validation samples are genuinely separate [30,31]. In small experiments, by contrast, additional model complexity can convert orderly treatment spacing into apparently impressive fit without improving generalization. Data-assimilation and inverse-model approaches offer substantial benefits when observations are sufficiently rich [27,28], but a low-parameter equation remains useful as a benchmark for judging whether that complexity earns a predictive gain.

Laboratory-to-model studies also illustrate the value of richer validation data. Ennazii et al. combined repeated measurements and two-phase modeling to examine open-channel bed erosion and bed evolution [44]. Improved physical modeling of confluences has similarly shown that laboratory boundary conditions can shape how well results transfer to field settings [45]. Those studies point to the next step for the present model: external validation should come from new independent runs, not from treating additional points within an existing bed survey as independent evidence. Until such runs exist, LOOCV provides a transparent internal stress test rather than proof of field generality.

3.4 Nondimensional interpretation

The particle-densimetric formulation was $d_s/d=-17.873+6.899Fr_p$. On the normalized response scale, R^2 reached 0.984, and Figure 4 shows a nearly linear increase of d_s/d with Fr_p over the observed range of 3.326–10.401. However, back-transforming predictions to centimetres reduced the fitted R^2 to 0.913, with RMSE=0.293 cm and MAE=0.258 cm. Under LOOCV, the back-transformed model produced R^2=0.850 and RMSE=0.385 cm. That RMSE is only 0.009 cm lower than the additive Q–d model, a difference smaller than the practical uncertainty associated with the source records and bed measurements.

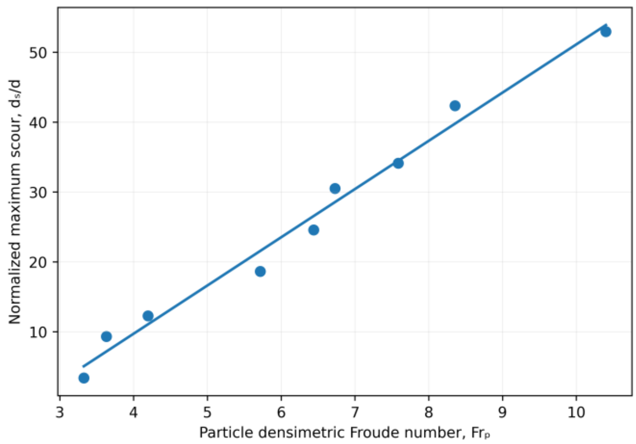

Figure 4. Normalized maximum scour (d_s/d) as a function of particle densimetric Froude number, with fitted relation $d_s/d=-17.873+6.899Fr_p$.
Source: experimental data and model results.

The distinction between ratio-scale and dimensional performance is essential. Grain size appears in the denominator of d_s/d and also enters Fr_p, so part of their strong association arises from shared mathematical structure. Dimensionless variables remain valuable because they can reveal physically meaningful combinations of forcing and resistance, and recent work advocates physics-informed dimensional reduction before high-flexibility modeling [29]. Yet a larger R^2 on a transformed scale is not, by itself, evidence of superior predictive utility. In this dataset, the fair comparison is the centimetre-scale cross-validated error, for which the nondimensional and additive models are effectively tied.

The reported Fr transition also deserves a measured interpretation. A beam-type sabo-dam study showed that changes in geometry and slope can shift Froude conditions while altering sediment-retention performance [34]. Reinforced porous deflectors have likewise been shown to reduce local velocity around bridge piers [25]. Those configurations contain deliberate flow-control structures, whereas the present bed does not. Their relevance lies in demonstrating how sensitive sediment response can be to changes in hydraulic regime; they should not be used to transfer a local-scour equation into the current unobstructed setting.

3.5 Physical meaning, practical scope, and limitations

Taken together, the results support a simple physical reading. Higher discharge increased the energetic capacity of the flow, and finer sediment reduced the resistance of the bed, so both manipulations moved the system toward deeper and more spatially extensive degradation. The progression from a deposition-dominated grid to 100% negative bed change is particularly important because it links the modeled maximum to the broader morphology. The same forcing–resistance logic is visible across other mobile-bed settings: downstream sediment deficits can intensify channel erosion [1], high-magnitude events can expand incision across a channel network [2], and bed roughness can evolve with sediment transport and surface organization [11]. The present experiment isolates that logic in a small controlled matrix.

At the same time, bulk velocity is not an independent causal variable here; it changes with the imposed discharge, the evolving bed, and the hydraulic state. This distinction is illustrated by experiments in which an added hydraulic resistance element changes velocity and sediment-related behavior. Akmal et al., working in the Krueng Aceh River and laboratory systems, showed that water-hyacinth structures substantially reduced velocity and increased hydraulic residence time [46]. Nurizkitha et al. similarly found that a porous deflector reduced velocity near a bridge-pier setting [25]. These studies concern different mechanisms, but they reinforce a general point: velocity is a system response to boundary conditions and resistance. For the present factorial experiment, Q and d remain the more defensible primary predictors because they were specified as treatment variables.

The model should therefore be used only within its calibration envelope: a 9 m laboratory flume, a 1,440 s run duration, Q=0.0026–0.0045 $m^3 s^{-1}$, and d=0.85–2.36 mm. It is not appropriate for bridge-foundation design, culvert protection, field-scale river prediction, or extrapolation to substantially different sediment gradations. Structure-specific studies repeatedly show that local scour depends on geometry and the local flow field [19,21]. The value of the current equation is instead as an interpolation rule and as a quantitative baseline for a second-generation experiment.

A further implication of the spatial record is that maximum scour and the scoured-point percentage carry different information and should not be substituted for one another. Two conditions can have similar maxima yet differ in how much of the measured bed has degraded. In this experiment, for example, a 2.9 cm maximum occurs under more than one treatment combination, but the surrounding distribution of negative values is not identical. This matters for engineering interpretation because a local extreme is relevant to clearance or embedment, whereas widespread degradation changes the hydraulic boundary over a larger part of the reach. The present study therefore retains the maximum as the response used in the compact model while using the full observation grid to judge whether that response is representative of a broader morphological state. The approach also avoids the opposite error of averaging away the deepest location, which would understate the local bed response.

That second experiment should prioritize true replication and richer hydraulic measurements. Independent repeat runs at selected low, intermediate, and high forcing states would provide an estimate of run-to-run variance, permitting a defensible test for curvature or Q×d interaction. Repeated laser, photogrammetric, structured-light, or acoustic bed surveys could replace reliance on a single end-of-run surface and support scour volume, bedform migration, and spatial autocorrelation analyses. Modern acoustic Doppler approaches can resolve river hydromorphodynamics at much higher temporal and spatial density [36], while open-channel sediment experiments and numerical models show that non-uniform gradation and three-dimensional transport structure can materially affect morphology [17,43].

The cross-validation results define a practical uncertainty scale for future testing. An RMSE of about 0.39 cm means that new flume observations within the same treatment envelope should not be expected to fall exactly on the fitted plane. A confirmatory experiment should therefore be designed to detect differences larger than this internal prediction error and should include repeated runs to separate model miss from run-to-run variability. This would also permit a more defensible assessment of whether the apparently stronger relative grain-size effect at low discharge reflects a real interaction or simply the arithmetic consequence of a small baseline scour value. In that sense, the present model is most useful as a quantitative experimental hypothesis: it specifies expected response direction, approximate effect size, and a cross-validated error against which a new dataset can be compared.

Near-bed turbulence and boundary shear should also be measured directly rather than inferred from an uncertain calculation chain. Numerical analysis confirms the central role of bed shear in rectangular open-channel flow [32], while mobile-dune experiments connect coherent turbulent events to entrainment and scour development [14]. A verified hierarchy could then compare the operational Q–d model with models based on shear velocity, Shields-type parameters, Fr_p, or measured turbulence metrics. Such a hierarchy would answer a more useful question than whether one regression has the highest fitted R^2: which added measurements materially improve out-of-sample prediction?

The source-data audit is the main limitation on the present numerical coefficients. Two pairs of 140-value bed tables are exact duplicates despite representing different treatment combinations, and several narrative maxima differ from the extrema in the corresponding tables. The largest discrepancy is 0.5 cm in the high-discharge/fine-bed condition, greater than the in-sample RMSE and comparable with the cross-validated error. The model therefore uses the table values consistently rather than mixing narrative and tabular sources. If original laboratory records establish corrected arrays or maxima, the coefficients and validation statistics should be recalculated. This limitation does not erase the monotonic treatment pattern, but it prevents the equation from being presented as a final design law.

Other limitations are structural to the experiment. There are only nine independent treatment conditions, bed topography is available only at 1,440 s, and the sediment is represented by nominal diameter rather than complete gradation, packing, or armoring descriptors. Open-channel studies show that grain-size distribution can alter transport organization [7] and that sediment composition changes suspension and erosion dynamics [8,9]. Consequently, the current results establish a stable directional relationship inside a controlled laboratory domain, not a universal entrainment threshold. Their strongest use is to define testable expectations for replicated experiments: increasing discharge should deepen and broaden degradation, while increasing grain size should suppress it, with the largest relative sensitivity expected near the low-forcing edge of the matrix.

4. Conclusion

Maximum bed scour in the unobstructed mobile-bed flume increased systematically with discharge and decreased with nominal grain size. Across the nine treatment combinations, maximum scour ranged from 0.8 to 4.5 cm, while the proportion of observation points with negative bed change increased from 19.3% to 100%. The spatial record therefore shows that increasing forcing was accompanied by a transition from mixed deposition and erosion to widespread degradation, not merely by a deeper isolated point.

The additive relation $d_s(cm)=1.272+0.883Q^*-1.037d^*$ provided the most useful balance of simplicity and predictive stability. It explained 93.5% of fitted variance and retained $R^2=0.843$ with RMSE=0.394 cm under leave-one-condition-out cross-validation. Standardized coefficients of +0.691 for discharge and −0.676 for grain size indicate nearly balanced effects in opposite directions over the tested ranges. The power-law alternative was less stable. The Fr_p-based model produced a very high normalized-scale fit, but after back-transformation its cross-validated error differed from the additive model by only 0.009 cm.

The resulting equation should be treated as an interpolation model for the tested flume conditions rather than a universal scour formula. Its principal contribution is the simultaneous quantification of discharge and grain-size effects, linked to the spatial expansion of bed degradation and evaluated with condition-wise cross-validation. Independent replication, full grain-size characterization, time-resolved bed surveys, and direct measurements of near-bed turbulence and shear are required before the model can be generalized. The documented inconsistencies among some source tables and narrative maxima also mean that the coefficients should be recalculated if corrected laboratory records become available.

Acknowledgments

The authors acknowledge the Water Resources Engineering Study Program, Faculty of Engineering, Universitas Muhammadiyah Makassar, and the laboratory staff and technicians who supported the open-channel experiments, hydraulic measurements, and bed-change observations.

Declarations

Declaration of generative AI and AI-assisted technologies in the manuscript preparation process. During the preparation of this manuscript, the authors used ChatGPT (OpenAI) to assist with language editing, manuscript organization, and consistency checking. The authors reviewed and revised the resulting text and take full responsibility for the content of the published work.

CRediT authorship contribution statement. Soemitro Emin Praja: Conceptualization; Methodology; Investigation; Data curation; Formal analysis; Validation; Visualization; Writing – original draft; Writing – review & editing. **M. Nurhidayat,** and **M. Agusalim**: Methodology; Investigation; Resources; Validation; Supervision; Writing – review & editing. **Asran**: Investigation; Data curation; Validation; Visualization; Writing – review & editing.

Funding. This research received no specific grant from funding agencies in the public, commercial, or not-for-profit sectors.

Declaration of competing interest. The authors declare that they have no known competing financial interests or personal relationships that could have appeared to influence the work reported in this paper.

Data availability. The hydraulic and bed-elevation measurements supporting the findings are held by the corresponding author and may be made available on reasonable request after reconciliation of the original laboratory records and any applicable institutional requirements.

References

[1] Abbasov R, Yahyayev V. The impact of dams and sand-gravel extractions on the downstream channel deformations (in the example of the Goychay River). Sustainable Water Resources Management. 2024;10(2).
[2] Broner N, Laronne JB, Storz-Peretz Y. Influence of flood events on the response of steep and coarse-grained channels to base-level lowering in an arid setting. Journal of Hydrology. 2024;645.
[3] Chang KH, Wu YT, Wang CH, Chang TJ. A new 2D ESPH bedload sediment transport model for rapidly varied flows over mobile beds. Journal of Hydrology. 2024;634.
[4] Duan JG, Yu C, Ding Y. Numerical Simulation of Sediment Transport in Unsteady Open Channel Flow. Water (Switzerland). 2023;15(14).
[5] Zerihun YT. Numerical Modeling of Sediment Transport and Bed Evolution in Nonuniform Open-Channel Flows. Archives of Hydroengineering and Environmental Mechanics. 2024;71(1):1-26.
[6] Liu C, Fu S, Li Z, Zhang Z, Zeng J. Effects of sediment characteristics on the sediment transport capacity of overland flow. International Soil and Water Conservation Research. 2023;11(1):75-85.
[7] Sen S, Hossain S, Ghoshal K. Distribution of non-uniform particles in an open channel flow from the concept of mixing length. Sedimentary Geology. 2022;440:106242.
[8] Yao P, Su M, Wang Z, van Rijn LC, Stive MJF, Xu C, Chen Y. Erosion Behavior of Sand-Silt Mixtures: Revisiting the Erosion Threshold. Water Resources Research. 2022;58(9).
[9] Qiao Z, Chen Y, Yao P, Su M, Stive M, Ren L, Wang Z. Suspension dynamics of sand-silt mixtures: Experimental insights and modelling implications. Journal of Hydrology. 2025;661.
[10] Ikhsan C, Permana AS, Negara AS. Armor Layer Uniformity and Thickness in Stationary Conditions with Steady Uniform Flow. Civil Engineering Journal (Iran). 2022;8(6):1086-99.
[11] de Menezes D, Borges ALO. Bed roughness in gravel-bed rivers: Channel-scale responses to flow and sediment dynamics. Advances in Water Resources. 2025;206.
[12] Canelas OB, Ferreira RML, Cardoso AH. Hydro-Morphodynamics of an Open-Channel Confluence With Bed Discordance at Dynamic Equilibrium. Water Resources Research. 2022;58(1).
[13] Aghazadegan A, Shokri A. Three-dimensional numerical simulation of mixing patterns at open channel confluences. Water Science and Engineering. 2025;18(2):236-46.
[14] Behera PK, Deshpande V, Kumar B. Dynamics of turbulent flow over mobile dune. Flow. 2025;5.
[15] Behera PK, Deshpande V, Kumar B. Morphodynamics of mobile dunes with downward seepage. Physics of Fluids. 2025;37(2).
[16] Li J, Xu N, Wang H, Fu D, Liu X, Wu W. Experimental investigation of the interconnections between turbulent structure and scouring topographic characteristics. Frontiers in Environmental Engineering. 2023;2.
[17] Malasani GC, Kantharaj M, Chandra V. Experimental study of suspended sediment transport at river confluence. Journal of Hydrology. 2026;671.
[18] Devi G, Kumar M. Experimental study of the local scour around the two piers in the tandem arrangement using ultrasonic ranging transducers. Ocean Engineering. 2022;266:112838.
[19] Alasadi LAR, Khlif TH, Hassan FA. Experimental investigation for the local scour around V-shaped spur-dikes. Scientific Review Engineering and Environmental Sciences. 2023;32(1).
[20] Murtaza N, Khan ZU, Khedher KM, Amir RA, Khan D, Salem MA, Alsulamy S. Mitigating scour at bridge abutments: An experimental investigation of waste material as an eco-friendly solution. Water. 2023;15(21):3798.
[21] Cely Calixto NJ, Galvis Castaño A, Carrillo Soto GA. Evaluation of Local Scour along the Base of Longitudinal Training Walls. Water (Switzerland). 2023;15(22).
[22] Chibana T, Quiocho R, Watanabe K. Role of Grain Size Distribution and Pier Aspect Ratio in Scouring and Sorting around Bridge Piers. Water (Switzerland). 2022;14(13).
[23] Chen F, Yang W, Liu F, Zhu L, Sun Z. Experimental Study of Sediment Incipient Velocity and Scouring in Submarine Cable Burial Areas. Water (Switzerland). 2025;17(9).
[24] Baharuddin A, Karim N, Ali MY, Latif S. Investigasi eksperimental pengendalian gerusan pilar jembatan menggunakan deflektor arus bawah air berpori. Journal of Green Complex Engineering. 2026;3(2):83-94.
[25] Nurizkitha IZ, Karim N, Al Imran H, Latif S. Efektivitas deflektor silinder pori bertulang dalam mengurangi kecepatan aliran di sekitar pilar jembatan. Journal of Green Complex Engineering. 2026;3(2):73-82.
[26] Bhat NUH, Pahar G. Depth-averaged coupling of submerged granular deformation with fluid flow: An augmented HLL scheme. Journal of Hydrology. 2022;606.
[27] Roushangar K, Ghasempour R, Azamathulla HM. An inverse problem for modeling open channel flow with movable bed. Water Supply. 2023;23(1):222-36.

[28] Ahmed MA, Li SS. Efficient Data Assimilation Method for Optimizing Prediction of Flow Field and Sediment Transport in Open Channel. River Research and Applications. 2026;42(3):580-93.
[29] Chen H, Wang F, Huai W, Li S. Analogues of Π Theorem via Machine Learning for Hydraulic Conveyance Laws. Water Resources Research. 2025;61(8).
[30] Pandey M, Karbasi M, Jamei M, Malik A, Pu JH. A Comprehensive Experimental and Computational Investigation on Estimation of Scour Depth at Bridge Abutment: Emerging Ensemble Intelligent Systems. Water Resources Management. 2023;37(9):3745-67.
[31] Guan D, Li Z, Zheng H, Hong JH, Fazeres-Ferradosa T, Asumadu R. Prediction of maximum scour depth downstream of bed sills using integrated machine learning algorithms. Environmental Modelling and Software. 2025;192.
[32] Huang Y, Zhou X, Zhou W, Yao C, Zhou F. Numerical Analysis of Bed Shear Stress of a Rectangular Open Channel. Gongcheng Kexue Yu Jishu/Advanced Engineering Sciences. 2022;54(3):201-8.
[33] Curulli G, Penna N, Gaudio R. Improved formulation for the geometric characteristics of the scour hole and deposition mound caused by a rotating propeller jet on a mobile bed. Ocean Engineering. 2023;267.
[34] Yusuf M, Tongeng AB, Marupah M, Latif S. Analisis eksperimental pengaruh sabo dam tipe beam terhadap karakteristik aliran debris pada variasi kemiringan saluran. Journal of Green Complex Engineering. 2026;3(2):67-72.
[35] Barahimi M, Sui J. Deformation of vegetated channel bed under ice-covered flow conditions. Journal of Hydrology. 2024;636.
[36] Fleit G, Muste M, Baranya S, Kim D, Whaling A, McAlpin TO, You H. The acoustic-doppler current profiler (ADCP): A comprehensive tool for river hydromorphodynamics monitoring. Advances in Water Resources. 2025;206.
[37] Good R, Nguyen D, Bonakdari H, Binns A, Gharabaghi B. Effect of Skewness Orientation on Morphological Adjustments in Alluvial Meandering Streams. Water (Switzerland). 2024;16(6).
[38] Lee J, Marr J, Guala M. On Sediment Mass Flux Directionality Induced by Yawed Permeable Vanes under Near-Critical Mobility Conditions. Journal of Hydraulic Engineering. 2022;148(10).
[39] Trevisson M, Eiff O. Fine-Sediment Erosion and Sediment-Ribbon Morphodynamics in Coarse-Grained Immobile Beds. Water Resources Research. 2022;58(11).
[40] Hakim Safi W, Mohapatra PK. Effects of Bed Material and Downstream Flow Depth on the Evolution of Bed in a Right-Angled Open-Channel Confluence. Journal of Irrigation and Drainage Engineering. 2024;150(1).
[41] Li J, Yang C, Chen X. Numerical investigation of grain size effect on velocity-skewed oscillatory sheet flow. Physics of Fluids. 2024;36(8).
[42] Pandey A, Kantamaneni K, Behera PK, Deshpande V, Sarukkalige R, Rathnayake U. Linking Grain Size and Geospatial Indices: Sediment Transport Dynamics in the Ganga River at Varanasi, India. Earth (Switzerland). 2026;7(1).
[43] Deng J, Brousse G, Jodeau M. How to improve numerical modelling of gravel replenishment with non-uniform sediment? Proof of concept with a comprehensive experimental dataset. Advances in Water Resources. 2025;206.
[44] Ennazii AE, Beaudoin A, Ouchene R, Gomit G, Jarny S, Calluaud D. Study of Bed Erosion in an Open-Channel from Laboratory Measurements to Eulerian–Eulerian Two-Phase Modeling. Water (Switzerland). 2026;18(11).
[45] Li K, Yu Q, Ma X, Wang L, Nie R. An Improved Physical Model for Open Channel Confluences: Bridging the Gap Between Laboratory and Field Observations. Water Resources Research. 2025;61(10).
[46] Akmal A, Munawir M, Puteh MAF, Syauqi TM, Saputra H. Hydrological assessment of a water hyacinth (Eichhornia crassipes) filtration system for microplastic and water quality improvement in the Krueng Aceh River. Jurnal LINEARS. 2026;9(1):9-18.

This page is intentionally left blank.

Journal of Green Complex Engineering